

Chapter 2

Common Experimental Issues

R. Kutschke, M. Paulini

2.1 Introduction

This chapter will discuss the experimental issues which underlie B physics at CDF, DØ and BTeV. Many of these issues also apply to charm physics, which will also be discussed. The chapter will be painted in fairly broad strokes and the reader is referred to the subsequent chapters and to the experiments' own Technical Design Reports (TDR) [1] [2] [3] [4] for more details on specific experiments.

During Run II, the Fermilab Tevatron will collide counter-rotating proton p and anti-proton \bar{p} beams at a center-of-mass energy of 2 TeV. Some other design parameters of the Tevatron for Run II are summarized in Table 2.1. In rough terms there are three processes which take place at this energy and which are important to the design of a B physics experiment. These are the production of $b\bar{b}$ pairs, the production of $c\bar{c}$ pairs and all of the light quark and gluon processes which contribute to the background; the cross-sections for these processes are summarized in Table 2.2. There are no known processes which produce a single b or a single \bar{b} at a significant rate, only processes which produce pairs. Despite this, one usually talks about b production, not $b\bar{b}$ production. Similarly, there are important sources of $c\bar{c}$ production but not of single c or \bar{c} production. The theory behind the production of heavy quark pairs in $p\bar{p}$ collisions is discussed in chapter 9. There are, of course, many other interesting processes which occur, including top quark production, Higgs boson production and perhaps even the production of supersymmetric particles. The cross-sections for these processes, however, are small enough that they do not have any impact on how one designs a B physics experiment for the Tevatron.

After a $b\bar{b}$ pair is produced, it hadronizes to form pairs of b hadrons including B mesons, such as B_d , B_u , B_s , B_c , and b baryons such as Λ_b , Ξ_b , Ω_b , Ξ_{bc} , Ω_{cc} etc. All of these states decay weakly, with a significant lifetime and, therefore, with a significant decay length. Excited states of these b hadrons are also produced, all of which decay strongly or electromagnetically to one of the weakly decaying b hadrons. A similar picture exists for the hadronization of $c\bar{c}$ pairs into hadrons. Therefore the route to all of b and c physics goes through the weakly decaying states.

One shorthand which will be used in the following is,

$$\sigma_{BG} = \sigma_{tot} - \sigma_{c\bar{c}} - \sigma_{b\bar{b}}. \quad (2.1)$$

Quantity	Value
Center of Mass Energy	2 TeV
Peak Instantaneous Luminosity	$2 \times 10^{32} \text{ cm}^{-2} \text{ s}^{-1}$
Yearly Integrated Luminosity	2 fb ⁻¹ /year
Time between bunch crossings	396 ns for $\simeq 2$ years 132 ns afterwards
Luminous region	$(\sigma_x, \sigma_y, \sigma_z) = (0.003, 0.003, 30.) \text{ cm}$

Table 2.1: Tevatron parameters for Run II. The conversion from peak instantaneous luminosity to yearly integrated luminosity assumes that a year consists of 10^7 useful seconds, as discussed in Section 2.5.

Quantity	Value (mb)	Comment
σ_{tot}	≈ 75	Total hadronic cross-section including elastic, diffractive and inelastic processes.
$\sigma_{c\bar{c}}$	≈ 1	Charm pair production cross-section.
$\sigma_{b\bar{b}}$	≈ 0.1	Beauty pair production cross-section.
σ_{BG}	≈ 75	The chapter's short-hand for $\sigma_{tot} - \sigma_{c\bar{c}} - \sigma_{b\bar{b}}$.

Table 2.2: Approximate values of the cross-sections which are of interest to a B physics experiment using $p\bar{p}$ collisions at a center-of-mass energy of 2 TeV. The estimate for the total cross-section is from Ref. [5]. The estimate of $\sigma_{b\bar{b}}$ is discussed in Section 2.4.

This stands for the “background” cross-section; that is for the total hadronic cross-section with the $c\bar{c}$ and $b\bar{b}$ pieces excluded. The $c\bar{c}$ piece is treated separately because it is interesting to study in its own right and because it has a few critical properties which are more like b 's than background. At our current level of precision, $\sigma_{BG} \simeq \sigma_{tot} \simeq 75 \text{ mb}$ [5]. This includes elastic $p\bar{p}$ scattering, diffractive scattering and inelastic scattering. Because $\sigma_{BG} \simeq \sigma_{tot}$ many authors are are careless about distinguishing between the two.

Throughout this chapter, the z axis is defined to lie along the beam direction and quantities such as p_T are measured with respect to this axis. The variable φ is the azimuth around the z axis and θ is the polar angle relative to the z axis.

2.2 Separating b and c Hadrons from the Backgrounds

Inspection of Table 2.2 shows that the cross-section for b production is about 1.5 parts in 1000 of the total cross-section. Moreover, many of the B physics processes of interest have

product branching fractions of 10^{-6} or smaller.¹ Therefore one is often looking for signals of a few parts per billion of the total cross-section!

The signature which allows one to see this needle in a haystack is the lifetime of the b quark. The B_d , B_u and B_s mesons each have a lifetime τ of approximately 1.5 ps, or $c\tau = 450 \mu\text{m}$. When the momentum spectrum of the B mesons is folded in, the mean decay length of all produced B mesons is on the order of a few mm. Therefore almost all B mesons decay inside the beam pipe. The resolution on the decay length varies from one decay mode to another and from one experiment to another but typical values fall in the range of $50 \mu\text{m}$ to $100 \mu\text{m}$; therefore the B decay vertices will be well resolved and will be readily separated from the $p\bar{p}$ interaction vertex. The B_c , the weakly decaying b baryons and the weakly decaying charmed hadrons have somewhat shorter lifetimes [6], but most of them have a long enough lifetime that their decay vertices too will also be well separated from $p\bar{p}$ interaction vertex.

The myriad background processes, with their much larger cross-sections, do not produce particles which have this type of decay length signature. This brings us to the magic bullet: it is the presence of distinct secondary vertices which allows the experiments to extract the b and c signals from the background.

About 85% of all weakly decaying b hadrons decay into one charmed hadron plus long lived particles. Long lived particles include pions, kaons, protons, photons, charged leptons and neutrinos, all of which are stable enough to escape the interaction region and leave tracks in the detector. Some of these particles, such as the K_S^0 and Λ do decay but their lifetimes are very long compared to the those of the b and c hadrons.² About 15% of weakly decaying b hadrons decay into 2 charmed hadrons, plus long lived particles; the decay $B^0 \rightarrow D^{*+}D^{*-}$ is an example. And about 1% of all weakly decaying b hadrons decay into only long lived particles; the decay $B^0 \rightarrow \pi^+\pi^-$ is an example. Therefore a typical $b\bar{b}$ event has 5 distinct vertices, all inside the beam pipe: the primary $p\bar{p}$ interaction vertex, the two secondary B decay vertices and the two tertiary c decay vertices. On the other hand, many of the most interesting decays involve charmless decays of the b and a typical event containing one of these these decays has 4 vertices inside the beam pipe: the primary $p\bar{p}$ vertex, the vertex from the signal charmless b , and the b and c vertices from the other b (or \bar{b}) produced in the $p\bar{p}$ interaction.

To be complete, one more detail must be added to the description of typical $b\bar{b}$ events. For the running conditions anticipated for Run II, each beam crossing which contains a $b\bar{b}$ interaction will also contain several background interactions which contain no $b\bar{b}$ or $c\bar{c}$ pairs. This is discussed in more detail in Section 2.5.1. Fig. 2.1 shows a cartoon of a $b\bar{b}$ event with one charmless b decay. Throughout this chapter the word “event” should be understood to include all of the interactions within one beam crossing, both the signal and background interactions.

¹The product branching fraction is defined as the product of all of the branching fractions in a decay chain. An example of such a decay chain is $B_d \rightarrow J/\psi K^0$, $J/\psi \rightarrow \mu^+\mu^-$, $K^0 \rightarrow K_S^0$, $K_S^0 \rightarrow \pi^+\pi^-$. The branching fraction for the first decay is about 1×10^{-3} , but the product of all branching fractions in the chain is much smaller, about 2×10^{-5} .

²The one exception is the τ lepton but the branching ratio of $b \rightarrow c\tau\nu$ is small, $(2.6 \pm 0.4)\%$ [6].

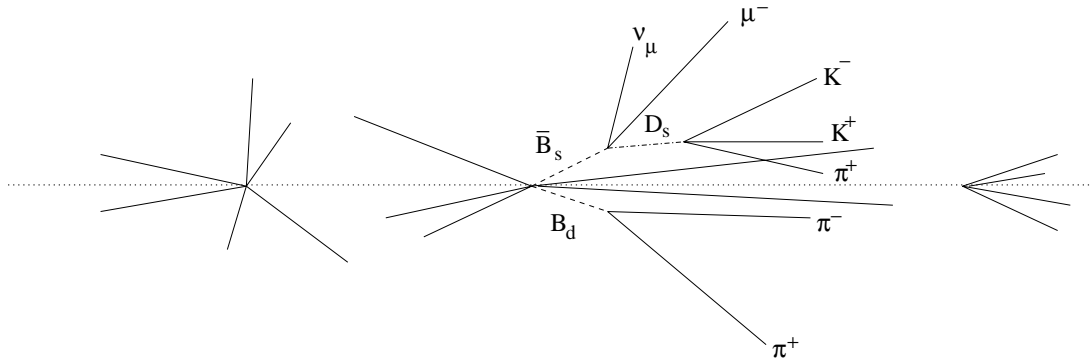


Figure 2.1: A cartoon of an interesting $b\bar{b}$ event at the Tevatron. In this beam-crossing the bunches undergo three independent primary interactions. The one in the middle produces a $b\bar{b}$ pair plus some other hadrons while the ones to either side are background interactions. In this event, one b undergoes a charmless decay while the other decays semileptonically to charm, which decays hadronically to light hadrons. The cartoon is meant to emphasize the topological properties of an event: it is not to scale and does not correctly represent the number of tracks in a vertex or the distribution of track directions.

Similarly, a typical $c\bar{c}$ interaction has three distinct vertices inside the beam pipe: the primary vertex plus two secondary vertices, which come from the decay of the two charmed hadrons. A typical beam crossing which contains a $c\bar{c}$ interaction will also contain a few background interactions.

In an event containing a $b\bar{b}$ or a $c\bar{c}$ pair, the stable daughters of the b and c hadrons usually have a large impact parameter with respect to the primary vertex. Because the beam spot is very narrow, roughly $30\ \mu\text{m}$ in diameter, these tracks will also have a large $r\varphi$ impact parameter with respect to the beam line. A track is said to be detached if the impact parameter, divided by its error, is large; this definition is used both for 2D and 3D impact parameters.

While the reconstruction of the full vertex topology of an event is a very powerful tool to reduce backgrounds, it is often too inefficient or too slow to be useful. In particular present computing technologies are too slow to allow full exploitation of the topology at trigger time. However a powerful trigger can be made by looking for the presence of a few detached tracks. All of CDF, DØ and BTeV have design triggers which make some sort of detachment requirement, with the sophistication of that requirement changing from one experiment to the next. BTeV exploits detachment at all trigger levels, including level 1, while the other experiments introduce detachment cuts only at higher levels. The reader is referred to chapters 3 to 5 for further details about the triggers of each experiment.

In addition to detachment, there are other properties which can be used to identify events which contain b quarks. For example, selecting events with one or two leptons of moderate to high p_T is an excellent way to select events containing $b\bar{b}$ pairs while rejecting background events. CDF and DØ have successfully used single lepton and di-lepton triggers, without any detachment requirement, to select events for their Run I B physics program. All of the Run II detectors plan some sort of lepton triggers, including single high p_T leptons, di-leptons and $\psi \rightarrow \mu^+\mu^-$ triggers. The experiments envisage some, but not all, of these

triggers also to include detachment information. For example, when evidence of detachment is present, one can lower p_T thresholds and still have an acceptable background suppression. But when detachment information is ignored, or unavailable, the triggers require higher p_T thresholds. Those triggers which do not include detachment information will provide a useful sample for calibrating the detachment based triggers.

One of the limitations of Run I was that the experiments could only trigger on b events with leptons in the final state. For Run II and beyond, both CDF and BTeV have triggers which rely only on detachment and which are capable of triggering all hadronic final states. The development of triggers which rely only on detachment is one of the major advances since Run I.

Because of their topological similarities to $b\bar{b}$ events, some $c\bar{c}$ events will also pass these triggers. Charm events, however, have properties which are intermediate to the b events and the background events: their decay lengths are shorter, their impact parameters smaller and their stable daughters have both a softer momentum spectrum and a softer p_T spectrum. Therefore the cuts which reduce the background to an acceptable level are much less efficient for $c\bar{c}$ events than they are for $b\bar{b}$ events. The CDF and DØ experiments do not expect that significant $c\bar{c}$ samples will pass their trigger and have not discussed a charm physics program. They can, of course, do some charm physics with the charm which is produced via B decay. BTeV, on the other hand, expects that a significant fraction of the events which pass their trigger, will contain $c\bar{c}$ events and they plan a charm physics program to exploit that data.

In summary, the long lifetimes of the weakly decaying b and c hadrons are the magic bullet which allow the b and c physics to be extracted from the background. At trigger time minimal cuts will be made on detachment and the offline analyses will make more complete use of the topological information. Various lepton based triggers, some with detachment requirements and some without, will form a second set of triggers.

2.3 Sources of Backgrounds

The most pernicious backgrounds are those which peak in the signal region and which can fake signals. One example of this is a true $B^0 \rightarrow K^+\pi^-$ being misreconstructed as a $B^0 \rightarrow \pi^+\pi^-$ decay; this results in a peak which is almost at the correct mass, with almost the correct width. This sort of problem is very mode specific and will be discussed, as needed, in the working group chapters.

A second class of backgrounds is combinatoric background within true $b\bar{b}$ and $c\bar{c}$ events, events which have the correct topological properties to pass the trigger. Suppose that one is looking for the decay, $B^0 \rightarrow D^-\pi^+$ followed by $D^- \rightarrow K^+\pi^-\pi^-$. All $b\bar{b}$ and $c\bar{c}$ events which produce a reconstructed $D^- \rightarrow K^+\pi^-\pi^-$ candidate have potential to produce background. If another track, perhaps from the main vertex, forms a good vertex with the D^- candidate this will be considered, incorrectly, as a B candidate. This sort of background will not peak near the B mass but it will produce background entries throughout the $D^-\pi^+$ mass plot, thereby diluting the signal. This sort of background can be reduced by

demanding that tracks which participate in a B candidate be inconsistent with the primary vertex. In addition, improved vertexing precision will reduce the number of random $D^- \pi^+$ combinations which form a vertex with an acceptable χ^2 .

There are many other background sources of secondary vertices and detached tracks: strange particles, interactions of particles with the detector material, misreconstructed tracks, multiple interactions per beam crossing, and mis-reconstructed vertices. While none of these backgrounds can create fake mass peaks at the B mass, they can dilute signals and they can overwhelm a poorly designed trigger.

At first thought one might summarily dismiss the strange hadrons as a source of background. After all, they typically have lifetimes 100 to 1000 times longer than those of the b hadrons; so only a small fraction will decay inside the beam pipe with a decay length typical of that for B decay. However they are produced about a few thousand times more frequently, a few per background interaction. Moreover the most probable decay time of an exponential distribution is zero, so some of the strange hadrons will have decay lengths of a few mm. There is a powerful countermeasure against most of the strange particle background: the trigger must ignore tracks with an impact parameter which is too large. One might worry that the contradictory requirements of a large detachment but a small impact parameter might leave no window to accept the physics. The answer is clear if one recalls the definition of detachment, an impact parameter divided by its error: make the error small. In practice the detectors have sufficiently good resolution that this background is reduced to acceptable level.

The strange hadrons have masses much less than the those of the b hadrons; therefore, an isolated decay of a strange particle is unlikely to be confused for a b decay. If however, another track, or tracks, pass close enough to the strange particle decay vertex that the reconstruction code incorrectly assigns that track to that strange particle's decay vertex, the combination can contribute combinatorial background beneath a B signal. This sort of background can be reduced by building a vertex detector with sufficiently high precision.

Another source of background comes from the interaction of the tracks with the detector and support materials. Photons can pair convert and hadrons can undergo inelastic collisions. There may be several of these secondary interactions for each primary $p\bar{p}$ interaction. Again, this sort of background can be suppressed, at the trigger level, by excluding tracks with too much detachment. And, in the offline analysis, one can exclude vertices which occur in the detector material. Having excellent resolution on vertex position is again the secret to background reduction.

Other sorts of interaction with the detector material includes Rutherford scattering and the tails of multiple Coulomb scattering. At the trigger level, the way to deal with these tracks is to make sure that the detachment cuts are large enough. At the offline reconstruction level, these tracks can often be rejected by cutting on the confidence level of the track fit.

Mis-reconstructed tracks are tracks which have incorrect hit assignments. The most direct way to deal with this problem is to ensure a sufficiently small occupancy in the detectors. For example, the upper limit for the long dimension of the BTeV pixels is set by such a study — if the pixels are too long then the two track separation degrades and

errors in pattern recognition result. This, in turn, creates false detached tracks. In the offline analysis, one can also reject mis-reconstructed tracks on the basis of a bad track fit confidence level.

Multiple interactions in one beam crossing are another source of background. Consider the case that two background interactions occur in the same beam crossing. In this case there are two chances that a background interaction might trigger the detector. But there is the additional complication that the trigger might fire based on some information from one vertex and some information from the other vertex. This last problem can be reduced by doing 3D vertexing in the trigger.

At the Tevatron the luminous region has a length of $\sigma_z \approx 30$ cm so it is reasonable to expect the triggers to behave acceptably with a few background interactions per beam crossing; most of the time the interactions will be well separated. When testing trigger algorithms it is important to measure how the trigger degrades with an increasing number of interactions per crossing. The trigger performance should degrade smoothly, without sudden drops.

The last background class is misreconstructed vertices, which includes both errors made when all of the tracks are well measured but also errors made when one of the tracks suffers from one of the diseases mentioned above. The solution is to ensure sufficient tracking precision that fake track rates are small and sufficient vertex precision that the rates for accidental vertices are small.

The above discussion has presented a number of factors which bound the detachment required at the trigger level from below and which bound impact parameter cuts from above. Using detailed simulations of their detector response, the experiments have shown that their proposed triggers will reduce these backgrounds to an acceptable level and that their detectors have enough rejection power to obtain an acceptable signal-to-background ratio during offline analysis. The common thread running through the discussion is that improved vertex resolution reduces every one of these backgrounds.

2.4 Basics of b Production Physics

At a $p\bar{p}$ collider, it is usually most convenient to describe particle production in terms of three variables, p_T , y and φ , where p_T is the transverse momentum of the particle with respect to the beam line, φ is the azimuth around the beam line and where the rapidity, y , is a measure of the polar angle, θ , relative to the beam line,

$$y = \frac{1}{2} \ln \left(\frac{E + P_{\parallel}}{E - P_{\parallel}} \right). \quad (2.2)$$

For historical reasons people sometimes work in units of pseudo-rapidity, η , instead of y ,

$$\eta = -\ln(\tan \theta/2). \quad (2.3)$$

For massless particles $\eta = y$ and for highly relativistic particles η approaches y . The utility of the variable η can be seen in Fig. 2.2, which shows the prediction of the PYTHIA Monte

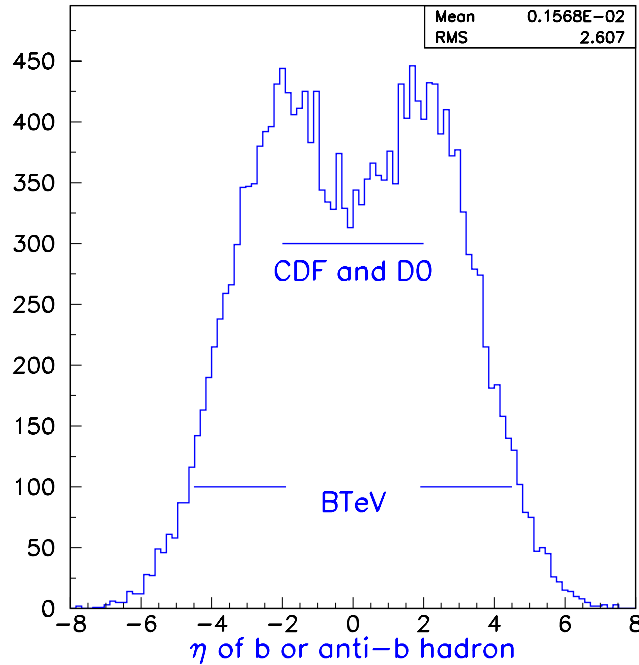


Figure 2.2: The production cross-section of B mesons vs η . The plot is from the PYTHIA event generator and does not contain detector effects. The horizontal lines show the regions of η which are covered by the three detectors. CDF and DØ do not cover all regions of η with equally quality; the barrel region, in which they make their best measurements covers approximately $|\eta| < 1.0$.

Carlo event generator for the production of b flavored hadrons as a function of η . The production is approximately flat in the central η region, falling off at large $|\eta|$, a general feature of particle production in hadronic collisions. The figure also shows the regions of η which are covered by the three detectors.

During Run I, both CDF and DØ studied the production of b quarks in $p\bar{p}$ collisions at a center-of-mass energy of 1.8 TeV. Both CDF and DØ have studied the central rapidity region $|\eta| < 1$ and DØ has also studied the forward region, $2.4 < y < 3.2$. The data of DØ are shown in Fig. 2.3. Both CDF and DØ find that the $b\bar{b}$ production cross-section in the central region is underestimated by the Mangano, Nason and Ridolfi (MNR) next-to-leading order QCD calculation [7] by a factor of more than two. The DØ data in the higher y^μ region is 3.6 ± 0.8 times higher than the QCD calculation.

When predicting their sensitivities for physics at Run II, CDF and DØ normalize their predictions to the cross-sections which they measured in Run I. Not only does BTeV not have previous data, there are no experimental data at all over much of the range of the BTeV acceptance, $1.9 \leq |\eta| \leq 4.5$. Instead BTeV uses the following procedure. When integrated over η and p_T , the QCD predictions shown in Fig. 2.3 predict a total $b\bar{b}$ production cross-section of $50 \mu\text{b}$. Since all of the experimental data is more than a factor of two above the theoretical calculations, BTeV estimates the total cross-section to be $100 \mu\text{b}$. BTeV then uses the predictions of PYTHIA to describe how the cross-section is distributed over p_T, η, φ .

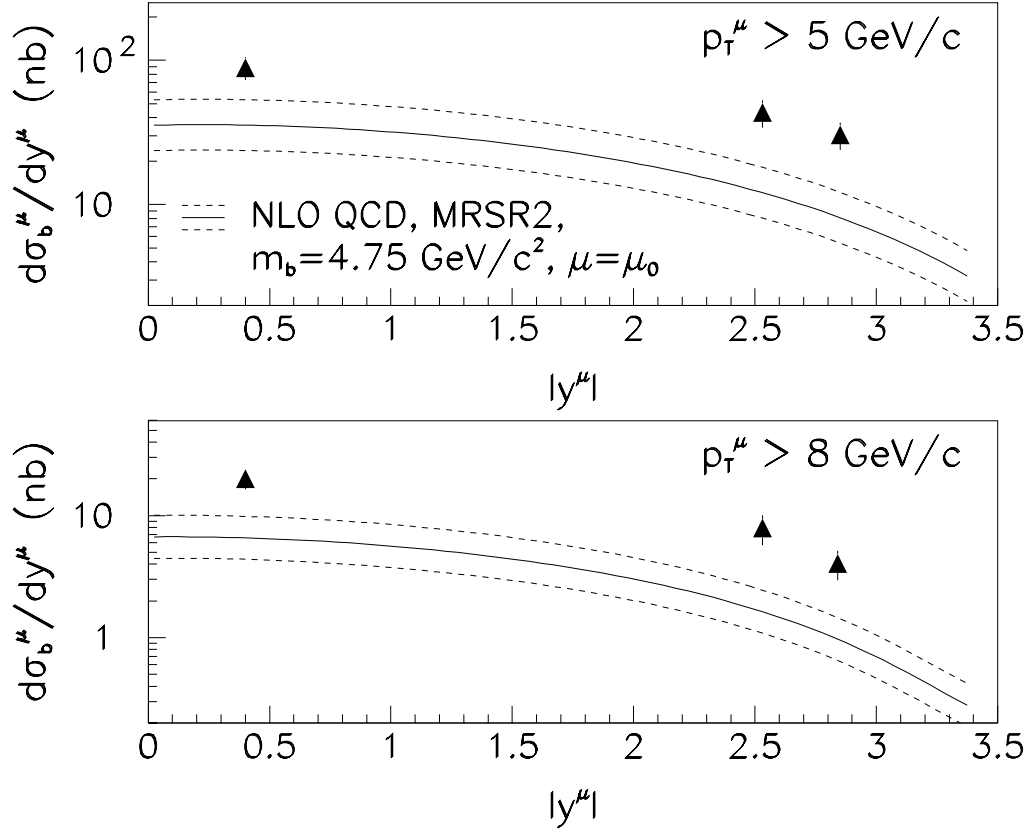


Figure 2.3: The cross-section for muons from b -decay as a function of the rapidity of the muon, y^μ , measured by $D\bar{O}$. The solid curve is the prediction of the next-to-leading order QCD calculation for a b -quark mass of 4.75 GeV. The dashed curves represent the estimated theoretical 1σ error band.

Within regions of phase space covered by CDF and $D\bar{O}$ PYTHIA has done a good job of describing the most important experimental correlations.

Other properties of $b\bar{b}$ production are illustrated in Fig. 2.4 through 2.6. Fig. 2.4 shows, for B mesons, the prediction of the PYTHIA event generator for the cross-section as a function of $\beta\gamma$ vs η . The figure shows that the bulk of the cross-section is concentrated in the central region and that forward going B mesons have a much higher momentum than do B mesons produced in the central region. This implies that in the forward region a greater fraction of the cross-section has long decay lengths, while in the central region there are more events to start with. The implications of this tradeoff will be discussed further in Section 2.8.1.

Fig. 2.5 illustrates another of the the properties of $b\bar{b}$ production, that b hadron and the \bar{b} hadron have an RMS separation of about one unit of η . The figure was made using generator level tracks from the PYTHIA event generator and shows the cross-section as a function of the polar angle of one B vs the polar angle of the other B . In a two-arm forward detector, such as BTeV, if one B is produced in a particular arm, then the other B is highly likely to be produced in the same arm. This is important for measurements

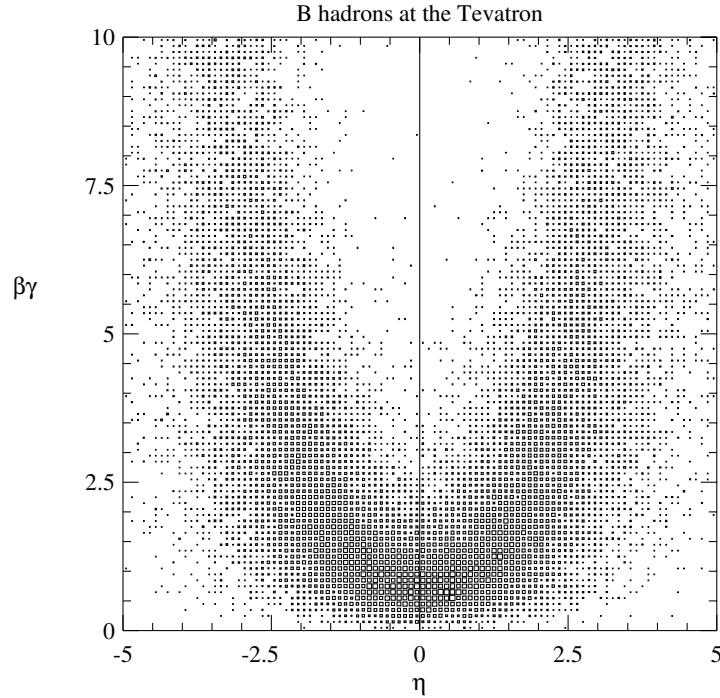


Figure 2.4: The production cross-section for B mesons as a function of $\beta\gamma$ and η plane. The plot is from the PYTHIA event generator and does not contain detector effects.

which make use of opposite side tagging (see Section 2.6). The choice of axes for this figure, θ rather than η , exaggerates this effect. Some other consequences of this distribution are discussed in Section 2.8.1.

Fig. 2.6 shows the azimuthal correlation between a b and its \bar{b} partner. The data are for $D\bar{O}$ events in which two muons are reconstructed, both consistent with coming from the decay of a B hadron. The horizontal axis is $\delta\varphi$, the difference in azimuth between the two muons. Since the selection criteria imply that the two B 's have a significant momentum, the muons tend to follow the B direction. Therefore $\delta\varphi$ is a measure of the difference in azimuth between the two b hadrons in the event. The band shows the prediction of MNR [7]. The b hadrons are preferentially produced back to back in azimuth and the gross shape is reproduced well by the model. It has already been noted that the MNR prediction underestimates the cross-section.

While the production of $b\bar{b}$ pairs is well described by perturbative QCD and knowledge of the structure functions of the proton, the hadronization, or fragmentation, of these quarks into the final state hadrons is described by models. These models are usually realized as computer codes for event generators, the most commonly used being PYTHIA [8], ISAJET [9] and HERWIG [10]. One of the properties which must be input to the event generators is the fraction of time that the b quark fragments into each of the allowed hadrons, B^- , \bar{B}^0 , \bar{B}_s , B_c^- or one of the b baryons. A recent measurement from CDF [11] gives, $f_u : f_d : f_s : f_{\text{baryon}} = 0.375 \pm 0.023 : 0.375 \pm 0.023 : 0.160 \pm 0.044 : 0.090 \pm 0.029$, with the assumption that $f_u = f_d$. If they release this assumption they obtain, $f_d/f_u = 0.84 \pm 0.16$. It is generally

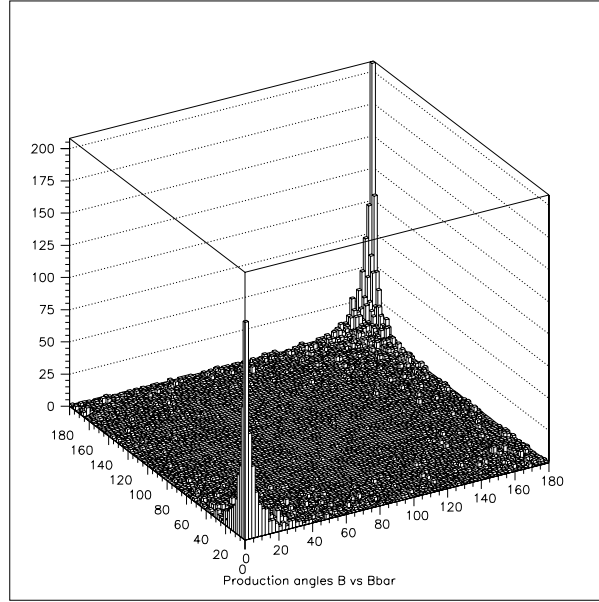


Figure 2.5: The production angle (in degrees) for the hadron containing a b quark plotted versus the production angle for a hadron containing \bar{b} quark. The plot is from the PYTHIA event generator and does not contain detector effects. One must be careful interpreting this plot since the natural axes are η , not θ .

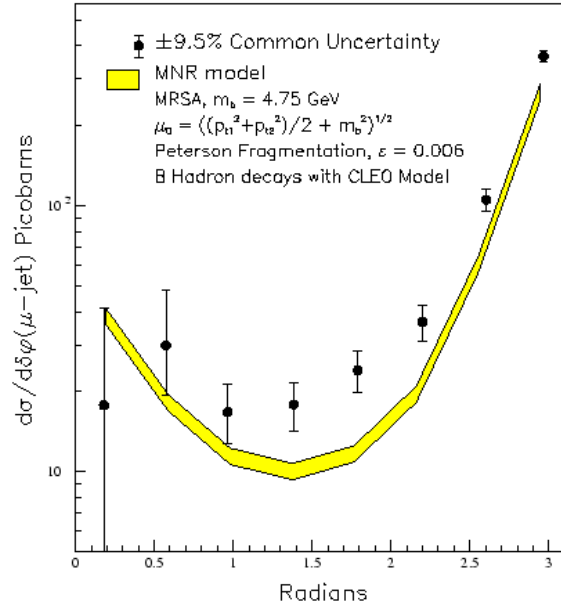


Figure 2.6: The differential $\delta\varphi$ cross-sections for $p_T^\mu > 9 \text{ GeV}/c$, $|\eta^\mu| < 0.6$, $E_T^{\bar{b}} > 10 \text{ GeV}$, $|\eta^{\bar{b}}| < 1.5$ compared with theoretical predictions. The data points have a common systematic uncertainty of $\pm 9.5\%$. The uncertainty in the theory curve arises from the error on the muonic branching fraction and the uncertainty in the fragmentation model.

-
-
1. The mechanisms which produce heavy flavors produce $b\bar{b}$ pairs but not single b or \bar{b} quarks. Similarly for charm production.
 2. The cross-section for $b\bar{b}$ production, integrated over all η and p_T , is about $100 \mu\text{b}$ and that for $c\bar{c}$ production is about 1 mb .
 3. The $b\bar{b}$ cross-section is approximately flat in η over the central region, and falls off at large $|\eta|$. See figure 2.2.
 4. b hadrons produced in the forward region have a higher momentum than those produced in the central region. See figure 2.4.
 5. The pair of b hadrons from one $b\bar{b}$ pair are approximately approximately back to back in φ and have an RMS separation in η of about one unit of η .
 6. The production ratio of $B_u : B_d : B_s : \text{baryons}$ is, $f_u : f_d : f_s : f_{\text{baryon}} = 0.375 \pm 0.023 : 0.375 \pm 0.023 : 0.160 \pm 0.044 : 0.090 \pm 0.029$ [11].
-
-

Table 2.3: Summary of the important properties of $b\bar{b}$ production.

presumed that, except for threshold effects, the fragmentation process is independent of the production process and is roughly independent of energy. For comparison the same production fractions measured at LEP and SLD are [12], $f_u : f_d : f_s : f_{\text{baryon}} = 0.401 \pm 0.010 : 0.401 \pm 0.010 : 0.100 \pm 0.012 : 0.099 \pm 0.017$. In both of these measurements, the production of B_c mesons is too small to be significant. In the standard event generators the choice of hadron species for the b quark is independent of the choice of hadron species for the \bar{b} quark. This cannot be exactly true since there is presumably some production via the $\Upsilon(4S)$ resonance, which decays only to $B^0\bar{B}^0$ or B^+B^- . Moreover the $B^0\bar{B}^0$ production from the $\Upsilon(4S)$ is coherent. While it is likely that these effects do occur, they can be safely ignored for purposes of this workshop. If there is enough resonant production to affect the physics results, the amount of such production can be easily measured with the Run II data.

The major points of this section are summarized in Table 2.3.

2.5 Production Rates and Interactions Per Crossing

The design value for the peak instantaneous luminosity during Run II is $2 \times 10^{32} \text{ cm}^{-2} \text{ s}^{-1}$. This specifies the luminosity at the start of a fill, when the beam intensities are greatest. As a fill progresses the instantaneous luminosity will drop. Also there will be shutdowns, both planned and unplanned, throughout the running period. The rule of thumb for converting the peak instantaneous luminosity to the yearly integrated luminosity is to assume that a year contains 10^7 seconds of running at the peak instantaneous luminosity. This is about one third of the actual number of seconds in a year, which accounts both for the drop in luminosity as a fill progresses and for a normal amount of down-time. Therefore a peak instantaneous luminosity of $2 \times 10^{32} \text{ cm}^{-2} \text{ s}^{-1}$ corresponds to $2 \text{ fb}^{-1}/\text{year}$.

Rate	$b\bar{b}$	$c\bar{c}$	Total
Interactions/s	2×10^4	2×10^5	1.5×10^7
Interactions/year	2×10^{11}	2×10^{12}	1.5×10^{14}
Interactions/crossing @ 396 ns	0.008	0.08	6
Interactions/crossing @ 132 ns	0.003	0.03	2

Table 2.4: Summary of production rates for $b\bar{b}$ pairs, $c\bar{c}$ pairs and total interactions for the design peak luminosity of the Tevatron during Run II, $2 \times 10^{32} \text{ cm}^{-2} \text{ s}^{-1}$ ($2 \text{ fb}^{-1}/\text{year}$). The interactions per bunch crossing are given twice, once for the bunch structure planned for early in Run II, 396 ns between bunch crossings, and once for the bunch structure planned for later in Run II, 132 ns between bunch crossings.

Given $\sigma_{b\bar{b}} = 100 \text{ } \mu\text{b}$ from Table 2.2, the above luminosities imply $b\bar{b}$ yield of 20,000/s or $2 \times 10^{11}/\text{year}$, about 3 to 4 orders of magnitude larger than the projected yields at the $e^+e^- B$ factories.

Given $\sigma_{tot} = 75 \text{ mb}$, from Table 2.2, a luminosity of $2 \times 10^{32} \text{ cm}^{-2} \text{ s}^{-1}$ implies a total interaction rate of $1.5 \times 10^7/\text{s}$. During the first few years of Run II the bunch structure of the Tevatron will be 396 ns between bunch crossings. At the design luminosity this would correspond to about 6 interactions per crossing but it is not expected that the design luminosity will be achieved this early in the run. After the first few years of Run II the bunch structure of the Tevatron will be changed to have 132 ns between bunch crossings. The purpose of this change is to allow an increase in luminosity while reducing the number interactions per beam crossing. At 132 ns between bunches, the design luminosity corresponds to about 2 interactions per bunch crossing.

The above discussion, along with the corresponding numbers for $c\bar{c}$ production, is summarized in Table 2.4.

The presence of multiple background interactions has many consequences for the design of the detector. It was already mentioned that the trigger must be robust against multiple background interactions in one beam crossing. The presence of multiple interactions must also be considered when designing the granularity of detectors to ensure that the occupancy is acceptably low.

2.5.1 The Distribution of Interactions Per Crossing

To a good approximation, if there are multiple interactions in one beam crossing, they are statistically independent of each other. This is not strictly true because, once the first interaction takes place, there are fewer beam particles left to participate in future interactions. However, in the limit that the number of particles per bunch is much larger than the number of interactions per crossing, each interaction can be treated as independent of all others.

Each of these independent interactions has some probability to produce a signal interaction and some probability to produce a background interaction. There are two, equivalent ways of looking at the distribution of signal and background interactions among the multiple interactions in one event. These equivalent ways are related to each other by the following identity. Given two independent Poisson processes, signal and background for example, the probability to observe n_1 interactions from the first process and n_2 interactions from the second process is,

$$\begin{aligned} P(n_1, n_2) &= \frac{(\mu_1)^{n_1}}{n_1!} e^{-\mu_1} \frac{(\mu_2)^{n_2}}{n_2!} e^{-\mu_2} \\ &= \left[\frac{\mu^n}{n!} e^{-\mu} \right] \left[f^{n_1} (1-f)^{n-n_1} \frac{n!}{n_1!(n-n_1)!} \right], \end{aligned} \quad (2.4)$$

where $f = \mu_1/\mu$ and $\mu = \mu_1 + \mu_2$. The first factor in [] is the Poisson probability to observe $n = n_1 + n_2$ interactions in total, while the second factor in [] is the binomial probability that the n interactions are split into n_1 from the first process and $n - n_1$ from the second process.

One can also show the general case, that the sum of M independent Poisson processes is itself a Poisson process with a mean $\mu = \mu_1 + \mu_2 + \dots + \mu_M$. In the general case, the factor multiplying the overall Poisson distribution will be a multinomial distribution, with the $M - 1$ independent parameters, $\mu_1/\mu, \mu_2/\mu, \dots, \mu_{M-1}/\mu$.

The two equivalent descriptions are: first, one can say that the total number of interactions within a beam crossing is Poisson distributed with a mean of μ and that within each beam crossing the interactions are distributed among the possible types according to a multinomial distribution. Second, one can say that there are M independent pieces to the cross-section and that each piece contributes to each beam crossing a Poisson distributed number of interactions with mean μ_M .

This second description is less well known but it allows one to more easily answer the following question: describe a typical beam crossing which produces a $b\bar{b}$ pair. For definiteness, consider the numbers summarized in Table 2.4 for the case of 132 ns bunch spacing; $\mu_{b\bar{b}} = 0.003$, $\mu_{c\bar{c}} = 0.03$, and $\mu_{BG} = 2.0$. Clearly most beam crossings will contain no $b\bar{b}$ pairs. An event which contains a typical $b\bar{b}$ pair will contain exactly one such pair and it will be accompanied by a Poisson distributed number of $c\bar{c}$ interactions with a mean of 0.03 interactions per crossing and by a Poisson distributed number of background interactions with a mean of 2.0 interactions per crossing.

2.6 Flavor Tagging

One of the main B physics goals of all three experimental programs is to make precision measurements of mixing mediated CP violating effects, some of which are discussed in chapter 6 of this report. Also, x_s has yet to be measured and that is interesting to measure in its own right. In order to perform any mixing related study it is necessary to know

whether a particular meson was produced as a $B^0(B_s)$ or as a $\bar{B}^0(\bar{B}_s)$. Making such a determination is called flavor tagging the B meson.³

Every tagging method sometimes produces the wrong answer and the effectiveness of flavor tagging is characterized by an effective tagging efficiency ϵD^2 , where $\epsilon = (N_R + N_W)/N$, $D = (N_R - N_W)/(N_R + N_W)$, N is the number of reconstructed signal events before tagging, N_R the number of right flavor tags, and where N_W is the number of wrong flavor tags. Another useful expression is $D = (1 - 2w)$ where $w = N_W/(N_R + N_W)$ is the fraction of wrong sign tags; from this expression it is clear that the tagging power goes to zero when the wrong sign tag fraction reaches 50%. Maximizing ϵD^2 is critical to the design of every experiment.

The quantity D is known as the dilution. This choice of nomenclature has the anti-intuitive result that a large dilution is good while a small dilution is bad. Never-the-less it is the standard nomenclature.

Tagging algorithms can be broken down into two classes, away side tagging and same side tagging. In away side tagging, or opposite side tagging, one looks at some property of the other b hadron in the event to determine its b quantum number. Since b quarks are produced as $b\bar{b}$ pairs, one can infer the flavor of the signal B meson. In same side tagging one uses the correlations which exist between the signal B meson and the charge of nearby tracks produced either in the fragmentation chain or in the decay of B^{**} resonances. For tagging B^0 mesons the correlation is with a charged pion, while for B_s mesons the correlation is with a charged kaon.

2.6.1 Away Side Tagging

The perfect away side tag would be to fully reconstruct the other b hadron in the event and to discover that it is a B^- or a Λ_b , neither of which undergoes flavor mixing. In this case one knows that the other b hadron contains a b quark and that the signal B meson must have been born with a \bar{b} quark. So the signal B is tagged as being born as a B^0 or as a B_s . In practice the efficiency for reconstructing a complete b hadron on the away side is much too small to be useful. Instead one looks for inclusive properties of b hadrons which are different from those of \bar{b} hadrons. Four such properties have been explored: lepton tagging, kaon tagging, jet charge tagging and vertex charge tagging.

Lepton tagging exploits the sign of the lepton in the decays $b \rightarrow X\ell^-$ compared to $\bar{b} \rightarrow X\ell^+$, where ℓ is either an electron or a muon. The branching fractions for these decays is roughly 10% into each of the e and μ channels. There is some dilution in this tag from the decay chain $b \rightarrow c \rightarrow X\ell^+$ compared to $\bar{b} \rightarrow \bar{c} \rightarrow X\ell^-$. However the two different sources of leptons have different kinematic properties and different vertex topology properties. So good separation between these two sources of leptons can be achieved. Another factor causes

³There is another, and very different concept called b tagging. If a lepton is part of a jet, and if the p_T of the lepton with respect to the jet axis is sufficiently large, then that lepton is most probably from the decay of a b quark within the jet. A sample of jets containing such a lepton will be heavily enriched in b jets. This technique was used extensively in Run I to tag samples of b jets which were used in the W boson and top quark physics programs. This technique is mostly of interest for top physics, not for B physics itself.

further dilution. In an ensemble of tags, the away side b hadron will be some mixture of B^+ , B^0 , B_s and several b baryons. The B^+ and the b baryons do not mix and so the observation of the sign of the lepton is a clear tag. However, 17.4% of the B^0 mesons will oscillate to \bar{B}^0 mesons before decaying [6] and will, therefore, give an incorrect tag. The B_s system, which is fully mixed, provides no tagging power at all.

Kaon tagging exploits the charge of the kaon in the away side decay chain, $b \rightarrow c \rightarrow XK^-$ compared with $\bar{b} \rightarrow \bar{c} \rightarrow XK^+$. Because of the large product branching fraction this tag has a much higher efficiency than lepton tags but historically has had worse dilution. With the improved vertexing power and particle identification capabilities of the of the Run II detectors one expects significantly improved dilutions. As with lepton tagging, there is tagging dilution from the mixing of the away side B^0 and B_s . It is often noted that a typical B_s decay contains two kaons of opposite strangeness and so contributes no power to kaon tagging. While this is true, one must remember that the B_s system is fully mixed and had no tagging power to start with.

A method called “jet charge tagging” exploits the fact that the sign of the momentum weighted sum of the particle charges of the opposite side b jet is the same as the sign of the charge of the b quark producing this jet. In a simple version, the jet charge Q_{jet} can be calculated as

$$Q_{\text{jet}} = \frac{\sum_i q_i (\vec{p}_i \cdot \hat{a})}{\sum_i \vec{p}_i \cdot \hat{a}}, \quad (2.5)$$

where q_i and \vec{p}_i are the charge and momentum of track i in the jet and \hat{a} is a unit vector along the jet axis. On average, the sign of the jet charge is the same as the sign of the b quark that produced the jet.

Vertex charge tagging involves reconstructing the full vertex topology of the away side. This does not necessarily constitute full reconstruction of the away side since the away side decay will usually contain π^0 's, photons, K_S^0 and K_L^0 . However these missing particles do not modify the charges of the remnant vertices. If the vertices have been correctly reconstructed, and if the away side secondary vertex has a charge of ± 1 , then the flavor of the away side b is known. If the charge of the away side secondary vertex is zero, then there is no tagging power. Also, if the away side tertiary vertex has charge ± 1 , one can infer the flavor of the away side b .

2.6.2 Same Side Tagging

Same side tagging exploits charge correlations between the a B^0 , or \bar{B}^0 , and the nearest pion in the fragmentation chain. Fig. 2.7 illustrates the idea behind the method.

One can think of the hadronization, or fragmentation, processes as pulling light quark pairs from the vacuum and forming hadrons from nearby quarks. In order to form a B^0 or a \bar{B}^0 meson the light quark pair which is nearest in the fragmentation chain to the initial heavy quark must have been a $d\bar{d}$ pair. This leaves a d or \bar{d} quark at the dangling end of the fragmentation chain. If the second nearest light quark pair is $u\bar{u}$ pair then the nearest meson in the fragmentation chain will be a π^- or π^+ , which can be used to tag the flavor of the initial b or \bar{b} . If the second nearest light quark pair is a $d\bar{d}$ pair then the nearest meson

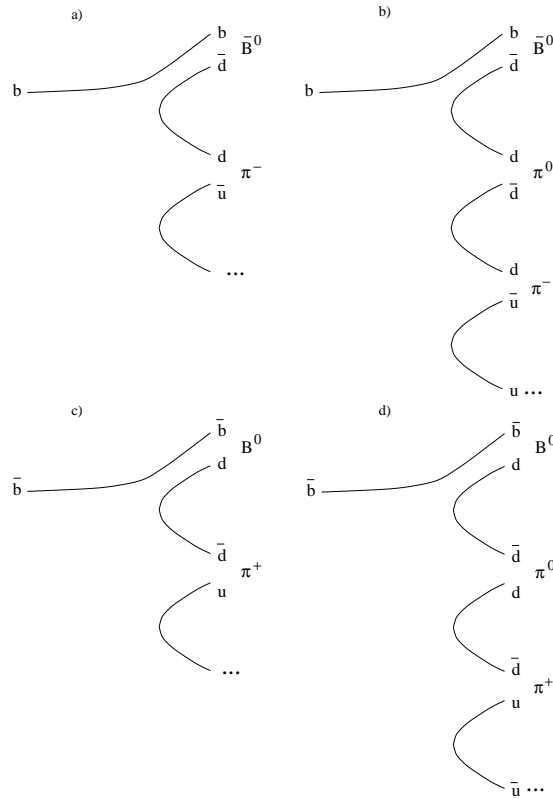


Figure 2.7: Four quark diagrams for the fragmentation of b and \bar{b} quarks to B^0 and \bar{B}^0 mesons. The charged pion which is nearest in the fragmentation chain to the B meson tags the birth flavor of the B meson. The notation \dots indicates that the fragmentation chain continues out of the picture.

is a π^0 , which itself has no tagging power. However the dangling end of the fragmentation chain remains a d or \bar{d} and, if the third nearest light quark pair is a $u\bar{u}$ pair, then the second nearest meson will be a π^- or π^+ which can be used as a flavor tag. The bottom line is that the charge of the nearest charged pion tags the birth flavor of the B^0 or \bar{B}^0 meson.

The question now is to discover an algorithm that will identify the charged pion that is the nearest charged pion in the fragmentation chain. CDF successfully developed such an algorithm in Run I. To select the same side tag pion, all tracks within a cone of radius 0.7 in $\eta\phi$ space, centered around the direction of the B meson, were considered. Same side tag candidate tracks were required to originate from the B production point (the primary event vertex), and were therefore required to satisfy $d_0/\sigma_{d_0} < 3$, where σ_{d_0} is the uncertainty on the track $r\phi$ impact parameter d_0 . This selection produced, on average, 2.2 same side tag candidate tracks per B candidate. String fragmentation models indicate that particles produced in the b quark hadronization chain have a small momenta transverse to the direction of the b quark momentum. CDF thus selected as the tag the track that had the minimum component of momentum, p_T^{rel} , orthogonal to the momentum sum of the track and the B meson.

The same fragmentation chain argument can be used to show that the nearest charged

kaon in the fragmentation chain can be used to tag the flavor of B_s and \bar{B}_s mesons. If the nearest kaon is a K^+ , then the meson is a B_s but if the nearest kaon is a K^- , then the meson is a \bar{B}_s . If, however, the nearest kaon is neutral, then there is no kaon tagging power because the nearest charged neighbor will be a pion. While there does remain a charge correlation with the nearest charged pion, the author is not aware of any work done to exploit this.

Compared with away side tagging methods, the same side tagging methods have a higher efficiency but a worse dilution. That is, they almost always find a candidate charged track but it is not always the correct one. Because of its high efficiency, same side tagging makes an important contribution to the total tagging power of an experiment.

2.6.3 Overall Tagging Strategy

The various methods described above have quite different properties. For example lepton tagging has a relatively low efficiency but a very good dilution. Same side tagging and jet charge tagging, on the other hand, are more efficient but have poorer dilutions. At CDF in Run I Kaon tagging was intermediate in both efficiency and dilution; better particle identification capability in the CDF Run II detector and in BTeV will significantly improve the dilution for this tag. The optimal tagging strategy is some method which involves all of the the tagging techniques. Any such strategy must account for the correlations among the away side tagging methods; same side tagging is statistically independent of all away side methods. One very simple strategy is to poll each method in order of decreasing dilution and to accept the first method that gives an answer. A more powerful idea is to combine all of the methods into an overall likelihood ratio, a linear discriminant or a neural net. The strategy employed by CDF in their Run I analysis of $\sin 2\beta$ is described in reference [13].

For further details one should consult the chapters for the specific experiments and the references therein.

2.7 The Measurement Error on Proper Decay Times

It is instructive to describe how one measures the proper decay time of a b hadron and to see that, for the decays of interest, the error on the proper decay time is, to a good approximation, independent of momentum.

To measure the proper decay time one reconstructs the primary interaction vertex at which the b hadron was produced and the secondary vertex at which the b hadron decayed. The proper decay time, t , is then given by $t = Lm/pc = L/\beta\gamma c$, where L is the decay length measured by the separation of the vertices, p is the measured momentum of the b hadron, m is the mass of the b hadron, c is the speed of light, and where β and γ are the usual Lorentz parameters for the b hadron. The uncertainty on the decay length contains contributions from the error on the primary vertex position, the error on the secondary vertex position and the error on the momentum of the b . In all three experiments the contributions from the position errors are much larger than those from the error on the momentum. And the

multiplicity of the primary vertex is usually much higher than that of the secondary vertex, making the error on the primary vertex position smaller than that of the secondary vertex; therefore the error on the proper decay time is dominated by the error on the position of the secondary vertex. The relevant part of the error on the secondary vertex is the projection of its error ellipse onto the flight direction of the b hadron. That is the dominant contribution to the error is just,

$$\sigma_t(\text{dominant contribution}) = \sigma_L^{(2ndry)} / (\beta\gamma c), \quad (2.6)$$

where $\sigma_L^{(2ndry)}$ is the contribution of the secondary vertex to the decay length.

There is one familiar exception to this rule. When using semi-leptonic decays to reconstruct the b , the momentum carried by the missing neutrals is poorly known and the error in the proper decay time has important contributions from the error in the momentum.

To understand how σ_t depends on momentum, consider two different instances of the decay $B^0 \rightarrow \pi^+\pi^-$. In the first case the B^0 has some definite momentum and the decay takes place at a particular point in some detector. Suppose that the momentum is large enough that both pions are boosted forward along the B flight direction in the lab. In the second case, the B^0 decays at exactly the same space point and with the same center-of-mass decay angles as in case 1, but it has a larger momentum. The decay products of this decay are then measured in the same detector. Further suppose that the detector is sufficiently uniform that each track from these two decays is equally well measured. The main difference between these two cases is that the lab frame opening angle between the two pions will be smaller in case 2 than in case 1. Because the opening angle is smaller, the point at which the tracks intersect is more poorly known. In particular the component of the vertex position along the b flight direction in the lab is more poorly known. This is purely a geometric effect. One result of this geometric effect is that the error on the secondary vertex position grows like γ ; that is $\sigma_L^{(2ndry)} \propto \gamma$. Plugging this into Eq. 2.6 gives $\sigma_t \propto 1/(\beta c)$. Therefore, for $\beta \simeq 1.0$, the error on the proper decay time is independent of momentum. This property has been exploited by experiments such as E687, E791, SELEX and FOCUS to make precision measurements of the charmed hadron lifetimes.

The above analysis holds approximately for multi-body decays of b hadrons. It will fail for very small boosts, in which case the decay products travel both forwards and backwards along the b flight direction. It will also fail if the decay products of the b hadron are slow enough that their errors are dominated by multiple scattering and not by the measurement errors in the apparatus.

The above analysis is only valid if the two decays are measured by the same detector. It is not useful for comparing two very different detectors; in that case there are no short cuts and one must compute the resolution of each detector.

2.8 Properties of a Good B Physics Detector

A detector for doing b and c physics at a hadron collider must have the following components, a high precision vertex detector, a tracking system giving excellent momentum resolution,

excellent particle identification (ID) capability, and a robust trigger integrated into a high bandwidth DAQ. And it is very desirable to have electromagnetic calorimetry so that modes containing photons and π^0 's can be measured.

It would also be useful to have hadronic calorimetry which is precise enough to reconstruct a K_L^0 . Because the K_L^0 has opposite CP quantum numbers to the K_S^0 , many tests of the weak interactions can be made by comparing exclusive final states which differ by substituting a K_L^0 for a K_S^0 . None of the three experiments, however, anticipate a significant ability to reconstruct K_L^0 mesons.

There are many other constraints on the detector design. For example, all of the detector elements must have sufficiently fine granularity to deal with the high multiplicities which occur in $p\bar{p}$ collisions. The detector must be able to deal with several such interactions in one beam crossing. And it is important to design the detector with as little mass as possible in the fiducial volume.

The three experiments have approached these challenges from different directions and with different constraints.

2.8.1 Forward vs Central

At first glance the most striking difference among the three detectors is that CDF and DØ are central detectors while BTeV is a forward detector. But there is a much more important distinction — BTeV is a dedicated B physics detector while CDF and DØ are multipurpose detectors whose primary mission is high p_T physics, including precision top quark physics, the search for the Higgs boson and the search for supersymmetric particles. Some of the constraints imposed on CDF and DØ are not intrinsic limitations of the central geometry; rather they are consequences of their optimization for a different spectrum of physics.

But there do remain some issues for which either the forward or central geometry has an advantage. First, BTeV has a harder particle ID job than either CDF or DØ because BTeV must identify tracks over a much wider range of momentum. However the forward geometry allows for a RICH detector which gives BTeV better overall hadronic particle ID. Second, BTeV has a somewhat higher efficiency for reconstructing the decay products of the second B in the event, given that the first B has already been reconstructed. The reasons behind this involve the interplay of production dynamics with the myriad constraints of detector design. Third, the forward geometry is more open than the central geometry, thereby simplifying the mechanical design and maintenance. In a central geometry, on the other hand, one unit of η is much more opened up in space than in the forward region. Since multiplicities are approximately uniform in η , this allows a device with coarse granularity to have the same multi-track separation power as does a fine granularity device in the forward region; this has advantages in channel count. Many of the advantages discussed in this paragraph are tied to available technologies and the situation might well change with new developments in detector technologies.

The B mesons produced in the forward region have higher momenta, and consequently longer decay lengths, than do those produced in the central region. Before drawing any

conclusions about the merits of forward produced B 's, one must take many other things into account. Not all B 's produced in the central region have low momentum and the ones which pass all analysis cuts have much higher momentum than the average B meson. There are more B mesons produced in the central region than in the forward region so central detectors can tolerate a smaller efficiency for their topological cuts and still have a comparable event yield. Higher momentum B mesons have poorer resolution on their decay vertex positions (see Section 2.7); this cuts the advantage of the highest momentum B mesons in forward detectors. The decay products of higher momentum B mesons undergo less multiple scattering than do those of lower momentum B mesons; this helps to improve resolutions. And the details of the detector design turn out to be the critical. The net result is that, after all analysis cuts, the early designs for the Run II CDF detector had a significantly poorer resolution on proper decay time than does BTeV. But with the addition of Layer-00, CDF now has a resolution on proper decay time, after all analysis cuts, which is comparable to that of BTeV.

At trigger time a different set of priorities is present. For example, in the lowest level of the BTeV trigger, the track fitting algorithms are crude and it is important that most B meson daughters are of high enough momentum that multiple scattering is a small enough effect to treat in a crude fashion.

The most important difference which arises from of BTeV being a dedicated experiment, while CDF and D0 are not, is in the trigger and DAQ systems. The BTeV trigger and DAQ system reconstructs tracks and makes a detachment based trigger decision at the lowest trigger level. Every beam crossing is inspected in this way. CDF and D0, on the other hand, must live within bandwidth budgets that were established before this sort of trigger was feasible. Therefore they have detachment information available only at level 2 and higher. For similar reasons their triggers have a higher p_T cut than does the BTeV trigger.

2.8.2 A Precision Vertex Detector

First and foremost it is necessary to have a high precision vertex detector. The importance of the vertex detector to the trigger has already been emphasized. Also, excellent resolution on proper decay time, which results from excellent vertex resolution, is necessary to study the time dependence of mixing mediated CP violating effects in the B_s system.

In a typical offline analysis chain, the vertex resolution appears to a high power. A typical candidate-driven $B^0 \rightarrow \pi^+\pi^-$ analysis might proceed as follows. First one finds a B^0 candidate and demands that the candidate B have a well defined vertex with a good χ^2 . Next, one must find the primary vertex of the $b\bar{b}$ interaction and care must be taken to ensure that this vertex is not contaminated by tracks from the other b hadron. One demands that the secondary vertex be well separated from the primary vertex. For some analyses it will be necessary to exclude B candidates if other tracks from the event are consistent with coming from the B decay vertex. Finally, one applies the available tagging methods. Each of these steps exploits the vertexing power of the experiment in a slightly different way. With so many steps, poor resolution has many chances to strike.

The vertex detector must have as low a mass as possible. Less mass implies less multiple

scattering and better vertex resolution. But a more important effect is that less mass reduces the number of interactions of signal tracks in the detector materials. When a signal track interacts in the detector, it is often unusable for physics and the event is lost. Examples include tracks which undergo inelastic hadronic interactions before reaching the particle ID device and photons which pair convert in the detector material.

A final consideration is the occupancy of the vertex detector. The occupancy is defined as the fraction of channels which are hit during a typical beam crossing. As the occupancy rises, the number of hit combinations which must be considered grows exponentially and pattern recognition becomes more difficult. If the occupancy is less than a few percent, offline pattern recognition is straight forward and standard algorithms compute sufficiently quickly. The driving factor in behind BTeV's choice of a pixel detector, rather than a strip detector, was to reduce the occupancy to approximately 10^{-4} . With this very low occupancy, even very simple, pattern recognition algorithms are efficient and produce low background levels; this allows their use at the lowest level of the trigger.

2.8.3 Tracking

The vertex detector must be supplemented by a tracking system with excellent momentum resolution. For most decay modes of interest, the mass resolution on the b hadron is dominated by the momentum resolution of the apparatus. If the mass resolution can be decreased by, say, 10%, one will get a 10% improvement in signal-to-background ratio without loss of signal efficiency. In a decay chain with several intermediate mass constraints this can add up.

Again it is important to minimize the mass in the tracking system and pay careful attention to the expected occupancy.

2.8.4 Particle ID

It is important to have an excellent particle identification with the ability to separate, with high efficiency, all of e, μ, π, K, p over a broad momentum range. All of the detectors have triggering modes which require lepton identification (lepton ID). Particle ID is also critical for reducing backgrounds which arise when one B decay mode is mistaken for another, such as $B_s \rightarrow D_s \pi$ being mistaken for $B_s \rightarrow D_s K$. Finally, excellent particle ID is crucial for a large ϵD^2 for kaon tagging.

All of the experiments have excellent lepton ID. Muon ID is done by finding tracks which penetrate a hadron shield. Electron ID is done by matching tracks in the tracking system with clusters of energy in the electromagnetic calorimeter.

BTeV is a dedicated B physics experiment and one of the factors driving the decision to build a forward spectrometer, not a central one, was that the forward geometry has room for a Ring Imaging Cherenkov counter (RICH). This provides the power to separate π, K, p from one another. On the other hand, the CDF and DØ detectors were originally optimized for high p_T physics, which did not require powerful π, K, p separation. Therefore the early

designs for the CDF and DØ Run II detectors did not include any device to do hadronic particle ID. Since then CDF has added a time of flight (TOF) system to perform π, K, p separation.

The reader is referred to the chapters 3 to 5 for further details.

2.8.5 Trigger and DAQ

In order to have a broad based B physics program, it is important to have an open trigger which is able to trigger on many B decay modes. This must be accompanied by a high bandwidth DAQ system which can move the data off the detector, move it between trigger levels and store it until a trigger decision is made.

The job of the trigger is to sort through the much more copious background interactions and extract a high purity b sample to write to tape. Ideally the trigger should be sensitive to some general property of b events, and have a high efficiency for a wide variety of B decay modes; it is not enough that the trigger performs well on some list of benchmark decay modes. This allows the greatest flexibility to explore ideas which are first thought of long after the trigger design was frozen. Of course one must verify that the trigger works well on the modes which we know now to be important.

A detachment based trigger meets all of these requirements; in particular it can trigger on all hadronic decay modes, a capability which was missing from the previous generation of experiments. A lepton based trigger, while missing the all hadronic modes, does meet many of the requirements and it will provide a redundant triggering method to calibrate the detachment based triggers.

The background rejection needed by the trigger is set by several things. Each level of the trigger must reduce the background to a low enough level that the bandwidth to the next level is not saturated. One must also consider the total amount of data which is written to tape; if too much data is written to tape, the main data reconstruction pass will take too long and the production of physics papers will be delayed. The cost of archival media is also an issue.

A final consideration is projecting results to higher instantaneous luminosities. As the luminosity increases, several limiting effects arise: one might reach the bandwidth limit of the DAQ system; one might exceed the amount of buffering at some level of the DAQ; the dead time might become too large. Once one of these limits is reached, the normal response is to raise some trigger threshold or to prescale some trigger. Typically one tries to sacrifice either the triggers which carry the least interesting physics or the triggers with poor signal to background ratios.

During an extended Run II but it is very likely that some of the B physics triggers will need to be modified to deal with the increased luminosity but it is difficult to project in detail what might need to be done. These decisions will depend, in part, on an understanding of backgrounds which is not yet available. Depending on the characteristics of the backgrounds, the trigger efficiency for some B physics channels may be unaffected while the trigger efficiency for other B physics channels may drop significantly.

The collaborations have concentrated their B physics trigger simulations on the conditions which will be present early in Run II, up to a luminosity of around $2 \times 10^{32} \text{ cm}^2\text{s}^{-1}$. So they have decided not to present projections for integrated luminosities of 10 and 30 fb^{-1} .

2.8.6 EM Calorimetry

A good electromagnetic calorimeter (EMcal) is necessary for the reconstruction of decay modes which contain final state photons and π^0 's. It is also necessary for electron ID, which can be used in triggering, in flavor tagging, in many searches for physics beyond the standard model.

There is one high profile decay mode for which the EMCal is critical, the analysis of the Dalitz plot for the decay $B^0 \rightarrow \pi^+\pi^-\pi^0$, a mode which measures the CKM angle α . The $\Upsilon(4S)$ machines are rate limited and are likely not to have sufficient statistics to make a definitive measurement of this quantity. The Tevatron detectors have the rate and, provided the EMCal technology is good enough, the measurement can be done.

A final use for an EMCal is to help sort out strong interaction effects which are entangled with the weak interaction physics that is the main goal. It is most straightforward to disentangle the strong interaction effects when all isospin permutations of the final state can be measured. The classic example of this are the decays $B^0 \rightarrow \pi^+\pi^-$, $B^0 \rightarrow \pi^0\pi^0$, and $B^+ \rightarrow \pi^+\pi^0$. While this complete set of decay modes is probably not measurable at the Tevatron, it illustrates the point.

All of the detectors have electromagnetic calorimetry. Both BTeV and CDF have discussed a B physics program which exploits it.

The EMCal system has a unique sensitivity to the issue of track density. As the number of tracks in the detector goes up, the occupancy of the calorimeter goes up. In the case of the tracking detectors one can compensate for high occupancy by making a more granular detector. This works because each track usually makes a small, localized signal in a tracking detector. In the case of a calorimeter, showers are extended objects which, by design, deposit energy in neighboring crystals or cells. Increasing the granularity of the detector will not make the showers any smaller. One can compensate for high occupancy by choosing calorimeter materials in which showers are contained in a smaller volume; if such materials are available, have sufficient energy resolution and radiation tolerance, and are affordable, then they can be used to make a calorimeter which can tolerate higher multiplicities.

2.8.7 Muon Detector

The final major hardware component in a B physics experiment is a muon detector system. This provides muon identification (ID) for such purposes as flavor tagging, reconstruction of J/ψ candidates, reconstruction of semileptonic decays, and searches for rare or forbidden decays. These last two classes include modes such as $B^0 \rightarrow \mu^+\mu^-$ and $B^0 \rightarrow e^+\mu^-$. A second job of these system is to provide an element of the trigger system; in some cases this is a stand alone trigger element and in other cases it is used in conjunction with other detector components to make a trigger decision.

The basic design of a muon detector is an iron or steel shield, many hadronic interaction lengths thick, which absorbs hadrons. Muons which penetrate this shield are detected by some sort of wire chamber tracking detector, or perhaps a scintillator, placed behind the shield. When possible other detector components, such as calorimeters and flux returns are used as part of the shielding. In another variation, iron shielding can be magnetized to allow measurement of the muon momentum in the muon system alone. This gives several benefits: it allows one to design a muon based trigger with a well defined p_T cut and it allows better matching between tracks in the muon system and tracks in the main tracking system.

2.9 Software

The software used by CDF, DØ and BTeV can be thought of in four classes, event generators, the B decay code, detector simulation tools and reconstruction code. The three experiments use common tools for the first two classes of software but generally use their own, detector specific software for the last two classes. The one exception is the MCFast fast simulation package which was used by both BTeV and CDF. MCFast is described extensively in the BTeV TDR [4]. BTeV is a new experiment which has tools which are quite advanced for such a young experiment but which are still primitive on an absolute scale. After Run I, CDF and DØ embarked on a major retooling of their software infrastructure, which was incomplete at the time of the workshop. So all of the results presented here use preliminary versions of code. At the level of precision required for the studies performed at this workshop, all of these tools are good enough.

The event generators are programs which generate the physics of a $p\bar{p}$ interaction; its output is usually just a list of vertices and particles which come out of those vertices. These programs are typically the intellectual property of the theoretical physicists who developed the model which is implemented in the program. The generators used by CDF, DØ and BTeV are PYTHIA [8], ISAJET [9] and HERWIG [10]. Generally these programs are used only to predict the shapes of the differential cross-sections, not for the absolute cross-sections. CDF and DØ have tuned the parameters of their event generators to match their Run I data. BTeV, on the other hand, has no such data against which to tune the codes. Therefore BTeV is using the programs as is.

The event generators have been carefully developed to simulate the properties of $p\bar{p}$ collisions but much less care was taken in their model of how b hadrons decay. To circumvent this, the b and c hadrons produced by the event generators are handed to a separate code to simulate their decay. Until recently this code was the QQ code, which was developed and maintained by CLEO, and which contains their integrated knowledge about the decays of B 's and D 's. The BaBar collaboration also has such a program, EVTGEN which will soon replace QQ. The results of the workshop were obtained using QQ.

The next step in a typical simulation is to compute the detector response to the simulated events. All of the experiments have both a fast simulation program and a detailed simulation program. A typical fast simulation program uses a simplified and/or parameterized description of the detector response and directly produces smeared 4-vectors for the

tracks which were input to it. It may also declare that a track is outside of the fiducial volume and is not reconstructible. The output of the fast simulation can usually be used as is to perform the simulated analysis.

A typical full simulation is based on the **GEANT 3** program from CERN. This is a program which knows how to describe a detector by building it up from a library of known shapes. It also has extensive knowledge of the interactions of particles with materials. It takes tracks from the event generator and propagates them through the detailed description of the detector, at each step checking to see how the track interacted with the material. If a particle interacts in the detector material to produce new particles, those new particles are also propagate through the detector. If a shower starts in material, **GEANT 3** will follow the daughters through each stage of the shower, and deposit the energy of the shower in the appropriate detector cells. The output of this simulation is typically a list of pulse heights or arrival times for hits in individual detector cells. This information is then passed to the reconstruction program and the trigger simulation codes.

At the time of the workshop, the experiments were still evaluating at the **GEANT 4** program, the C++ based successor to **GEANT 3**.

CDF and DØ have data samples from Run I which can be used. Signal yields can be projected from the Run I signal yields by computing the ratio of efficiencies in the old and new detectors. This avoids the need to make assumptions about the total cross-section, as BTeV must do. CDF and DØ use background samples from Run I to estimate background levels in Run II. BTeV must rely entirely on simulations for this purpose.

The reconstruction code starts with raw hits, either from the detector or from a simulation of the detector, calibrates them, find tracks, fits them, finds showers, applies the particle ID algorithms and so on. The output of this step is the measured properties of tracks and showers, which can be used directly for physics analysis.

The trigger simulation codes start with the same raw hits as the reconstruction code. In some cases the codes emulate the trigger hardware and produce trigger decisions which should very closely represent the real trigger behavior. In other cases the simulation codes

For more details on the software of each experiment, consult their TDRs [1] [2] [3] [4] and chapters 3 to 5 in this report.

2.10 Comparison with e^+e^- Machines

For most of their lifetime the Tevatron experiments will be in competition with the detectors from the $\Upsilon(4S)$ e^+e^- factories, BaBar and Belle. The charm physics program of BTeV will also face competition from CLEO-c. While these programs are competition, they also complement the Tevatron program. Some precision measurements will be best done in the cleaner environment of e^+e^- : they have a well determined initial state, either pure $B^0\bar{B}^0$ or B^+B^- , with no additional tracks in the event. And the production of B mesons represents about 20% of their total cross-section, which greatly simplifies triggering and removes many trigger biases. Similar advantages hold for the open charm program at CLEO-c.

On the other hand, the Tevatron experiments have a significant rate advantage which give it the advantage for many rare decay modes and in those measurements which are statistically limited. Only the Tevatron experiments have access to the decays of the B_s and b baryons, which are necessary to complete the program of over constraining the CKM matrix. See, for example, the discussion of B_s mixing in chapter 8.

References

- [1] The CDF II Collaboration, R. Blair *et al.*, *The CDF II Detector Technical Design Report*, Fermilab-Pub-96/390-E. This Report may be found at the url: <http://www-cdf.fnal.gov/upgrades/tdr/tdr.html>.
- [2] The CDF II Collaboration, “*Update to Proposal P-909: Physics Performance of the CDF II Detector with an Inner Silicon Layer and a Time-of-Flight Detector*”, submitted to the Fermilab Director and PAC, 5 Jan 1999.
- [3] The DØ Collaboration, “The DØ Upgrade”, submitted to the Fermilab PAC August 1996, Fermilab Pub-96/357-E, <http://higgs.physics.lsa.umich.edu/dzero/d0doc96/d0doc.html>.
- [4] The BTeV Collaboration, “Proposal for an Experiment to Measure Mixing, CP Violation and Rare Decays in Charm and Beauty Particle Decays at the Fermilab Collider — BTeV”, Submitted to the Fermilab Director and PAC, May 2000. This report may be found at the URL: http://www-btev.fnal.gov/public_documents/btev_proposal/index.html
- [5] The CDF Collaboration, F. Abe *et al.*, Phys. Rev. D **50**, 5550 (1994).
The E-811 Collaboration, C. Avila *et al.*, Phys. Lett. **B445** 419 (1999).
- [6] The Particle Data Group, D. E. Groom *et al.*, The European Physical Journal **C15**, 1 (2000).
- [7] M. Mangano, P. Nason and G. Ridolfi, Nucl. Phys. **B373**, 295 (1992).
- [8] H. U. Bengtsson and T. Sjostrand, Comp. Phys. Comm. **46**, 43 (1987).
- [9] F. Paige and S. Protopopescu, Brookhaven National Laboratory Report BNL-37066 (1985) (unpublished).
- [10] G. Marchesini and B.R Webber, Nucl. Phys. **B310**, 461 (1988); Nucl. Phys. **B330**, 261 (1988);
I. G. Knowles, Nucl. Phys. **B310**, 571 (1988);
G. Abbiendi, *et al.*, Comp. Phys. Comm. **67**, 465 (1992).
- [11] The CDF Collaboration, T. Affolder *et al.*, Phys. Rev. Lett. **84**, 1663 (2000).
- [12] D. Abbaneo *et al.*, “Combined results on b hadron production rates, lifetimes, oscillations and semileptonic decays,” hep-ex/0009052.
- [13] The CDF Collaboration, T. Affolder *et al.* Phys. Rev. D **61**, 072005 (2000) [hep-ex/9909003].
- [14] The CDF Collaboration, F. Abe *et al.*, Phys. Rev. Lett. **75** 1451 (1995).
- [15] The DØ Collaboration, R. Abbott *et al.*, Phys. Rev. Lett. **74** 3548 (1995).

-
- [16] D. Fein, “Tevatron Results on b -Quark Cross Sections and Correlations”, presented at Hadron Collider Physics (HCP99), Bombay, January 1999.
- [17] The DØ Collaboration, B. Abbott *et al.*, Phys. Rev. Lett. **84** 5478 (2000) [hep-ex/9907029].
- [18] The DØ Collaboration, B. Abbott *et al.*, “The $b\bar{b}$ Production Cross Section and Angular Correlations in $p\bar{p}$ Collisions at $\sqrt{s} = 1.8$ TeV”, Phys. Lett. **B487** 264 (2000) [hep-ex/9905024].